Heat capacity of helium in cylindrical environments

S. M. Gatica,[1] E. S. Hernández,[1] and L. Szybisz[1,2]
[1]*Departamento de Física, Facultad de Ciencias Exactas y Naturales, Universidad de Buenos Aires, RA-1428 Buenos Aires, Argentina, and Consejo Nacional de Investigaciones Científicas y Técnicas, Buenos Aires, Argentina*
[2]*Laboratorio Tandar, Comisión Nacional de Energía Atómica, Av, Libertador 8250, RA-1429 Buenos Aires, Argentina*
(Received 12 December 2002; published 1 October 2003)

We perform a systematic investigation of the structure, elementary, and phonon excitations of quantum fluid ^{4}He adsorbed in the interior of carbon nanotubes. We show that the helium fluid inside the cylinder behaves exactly as in planar films on a graphite substrate, presenting the same kind of layering transition. This tendency is confirmed by the behavior of a single ^{3}He impurity diluted into adsorbed ^{4}He. We also present a simple description of the lowest excitation modes of the adsorbed fluid and compute the low-temperature contribution of the phonon spectrum to the specific heat, which displays the dimensionality characteristics reported in previous works.

DOI: 10.1103/PhysRevB.68.144501 PACS number(s): 67.70.+n, 65.20.+w, 67.60.−g, 67.90.+z

I. INTRODUCTION

In recent years a large amount of work has been devoted to study the adsorption of quantum fluids in confined geometries. Special attention have been paid to systems with cylindrical confinements[1–8] and, in particular, adsorption of liquid helium onto walls of carbon nanotubes offers a variety of interesting behaviors.[1] In Ref. 3, a new situation was identified, characterized by the presence of a sharp peak in the density profiles of the adsorbed fluid aligned with the central axis of the tube, which constitutes a possible realization of a one- or quasi-one-dimensional (Q1D) quantum fluid.[9–13] Quite recently, it has been shown that this restricted dimensionality makes room for the possibility of spin-zero sound driven by the attractive particle-hole interaction of liquid ^{3}He.[12,13]

In this work we shall examine in depth the nature of this new ''axial phase'' found in carbon nanotubes, performing a detailed examination of the structure and energetics of adsorbed ^{4}He as the number of adatoms increases, within the frame of finite-range density functional theory. Since the general shape of the equation of state (EOS) and density profiles for such systems was presented in Ref. 3, in this work we concentrate in the analysis of the excited states of the helium atoms and their role in the appearance of successive inner layers of the fluid. Furthermore, we shall evaluate the probability density of a single ^{3}He impurity adsorbed into the ^{4}He fluid. We shall also discuss some aspects of measurable thermal effects—i.e., the heat capacity—associated with phonon excitations in these fluids. In fact, a related problem has been previously addressed in Ref. 14, where a hydrodynamic description for acoustic modes with isotropic dispersion on a cylindrical surface was adopted, in order to examine the dimensionality crossover of the heat capacity from one to two dimensions in such environments.

This approach has been most recently extended to investigate the phonon modes and thermal response of fluids adsorbed on a spherical wall.[15] Moreover, several properties of the specific heat of a dilute, quasi-one-dimensional helium system have been recently studied,[11] and our interest here focuses on the superspinodal linear density regimes, where radial transverse motion of the adatoms comes into play.

The paper is organized in the following way. In Sec. II we analyze the structure and elementary excitations of the ^{4}He fluid in a single-wall carbon nanotube as well as the behavior of the ^{3}He impurity. Thermodynamic properties of the excitations are given in Sec. III, where we indicate the appearance of the collective branches provided by the random phase approximation (RPA) for fluid ^{4}He in a cylindrical environment and analyze their contribution to the specific heat in the phonon regime. Section IV is devoted to the summary and conclusions.

II. ELEMENTARY EXCITATIONS OF ^{4}He IN THE CYLINDRICAL ENVIRONMENT

In this work we adopt the Orsay-Trento (OT) density functional[16] and minimize the total energy of N_4 helium atoms, bound to a graphite tube of radius R_t and length $L(L \gg R_t)$ by a confining field $V_s(r)$, with respect to the radial density $\rho_4(r)$. The variational Euler-Lagrange equation in the mean field is of the form

$$\left[-\frac{\hbar^2}{2m}\nabla^2 + V[\rho_4(r)] - \mu_4 \right] \sqrt{\rho_4} = 0, \tag{2.1}$$

with μ_4 the chemical potential which guarantees particle number conservation, i.e.,

$$N_4 = 2\pi L \int r dr \rho_4(r), \tag{2.2}$$

and where the mean field $V[\rho_4(r)]$ includes the substrate potential. Having computed the ground-state self-consistent density $\rho_4(r)$ as a function of the linear density $n_4 = N_4/L$, one can tackle the spectral problem of the one-body Hamiltonian in cylindrical coordinates

$$H_4 = -\frac{\hbar^2}{2m}\left[\frac{1}{r}\frac{\partial}{\partial r}\left(r\frac{\partial}{\partial r}\right) + \frac{1}{r^2}\frac{\partial^2}{\partial \varphi^2} + \frac{\partial^2}{\partial z^2}\right] + V[\rho_4(r)]. \tag{2.3}$$

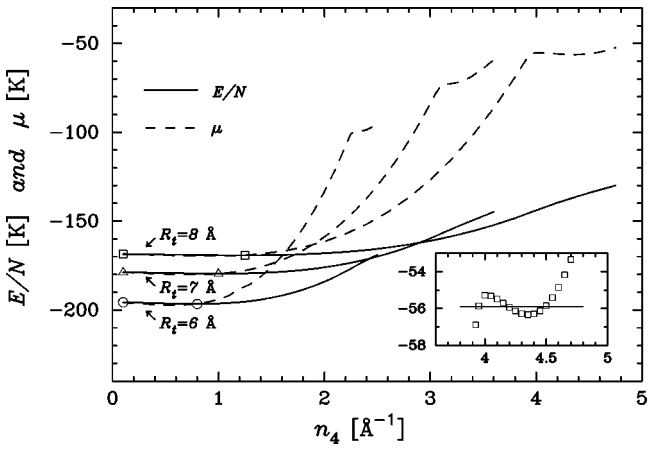

FIG. 1. Total energy per particle and chemical potential of helium atoms in cylinders of radii $R_t=6$, 7, and 8 Å as functions of linear density n_4. The inset shows the Maxwell construction for the tube with $R_t=8$ Å.

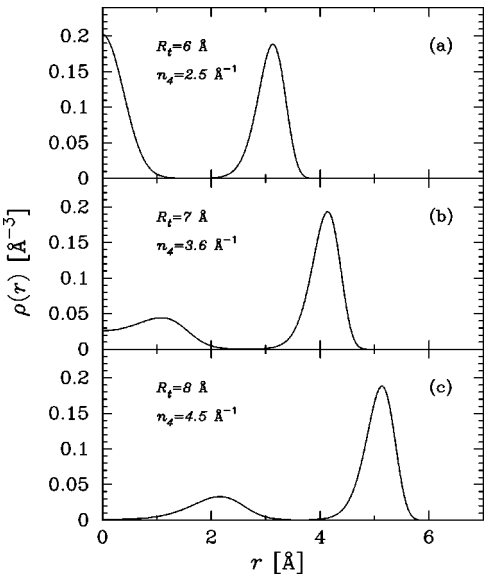

FIG. 2. Density of helium in the cylinders of Fig. 1. The linear densities correspond to a surface coverage $n_s=n_4/(2\pi R_{shell})$ of about 0.14 Å^{-1}.

The eigenvalue equation $H_4\Phi_{nlk}(r)=\varepsilon_{nlk}\Phi_{nlk}(r)$ can be solved for single-particle (s.p.) wave functions

$$\Phi_{nlk}(\mathbf{r})=f_{nl}(r)\frac{e^{i(kz+l\varphi)}}{\sqrt{2\pi L}} \tag{2.4}$$

and eigenenergies

$$\varepsilon_{nlk}=\varepsilon_{nl}+\hbar^2k^2/2m, \tag{2.5}$$

where the momentum-independent functions $f_{nl}(r)$ and the eigenenergies ε_{nl} satisfy

$$-\frac{\hbar^2}{2m}\left(f''_{nl}+\frac{f'_{nl}}{r}\right)+\left[V[\rho_4(r)]+\frac{\hbar^2l^2}{2mr^2}\right]f_{nl}=\varepsilon_{nl}f_{nl}. \tag{2.6}$$

The particular solution $\varepsilon_{00}=\mu_4$ and $f_{00}=\sqrt{2\pi\rho_4/n_4}$ corresponds to Eq. (2.1). Keeping in mind the shape (2.4) of the wave function, hereafter we shall denote as longitudinal and transverse motion, respectively, that associated with displacements along the axis of the tube (z motion) or along its radius (r motion).

We have solved Eq. (2.6) for various linear densities n_4 assuming a binding field of the form[17]

$$V_s(r,R_t)=3\pi\theta_s\epsilon\sigma^2\left[\frac{21}{32}\left(\frac{\sigma}{R_t}\right)^{10}M_{11}(r/R_t)-\left(\frac{\sigma}{R_t}\right)^4M_5(r/R_t)\right], \tag{2.7}$$

with $\epsilon=16.24$ K, $\sigma=2.74$ Å, $\theta_s=0.38$ Å^{-2}, and

$$M_n(x)=\int_0^\pi\frac{d\varphi}{(1+x^2-2x\cos\varphi)^{n/2}}. \tag{2.8}$$

The main results can be summarized as follows. Figure 1 displays the total energy per particle and the chemical potential as functions of the linear density n_4, corresponding to helium in tubes with radii 6, 7, and 8 Å . We visualize very clear jumps in the slope of the chemical potential at values of $n_4=2.23$, 3.1, and 3.93 Å^{-1}, which indicate transitions to configurations with more than one cylindrical shell adhered to the wall. The corresponding fluid patterns can be viewed in Fig. 2, which displays the radial density $\rho_4(r)$ as a function of the distance to the tube axis. The linear density n_4 has been chosen so that the surface coverage on the cylindrical shell, $n_s=n_4/(2\pi R_{shell})$, with R_{shell} the centroid of the peak close to the wall, takes values around 0.14 Å^{-2}. For these numbers of atoms the second maxima in the density profiles are well developed, and the fluid inside the tube tends to reproduce the layering sequence already encountered on flat graphite surfaces,[18–21] where the density profile exhibits oscillations with quasiperiod of about 3 Å. In the current geometry, this represents a sequence of concentric cylindrical shells; in the case $R_t=6$ Å, the second shell collapses into the so-called axial state, which constitutes a possible realization of a one- or quasi-one-dimensional quantum fluid. In Ref. 3, this new situation was identified as the axial regime; moreover, calculations of the adsorption isotherm for H_2 at zero temperature indicate that the axial one seems to be a true phase of the fluid adsorbed in a nanotube bundle, which could be reached after a sequence of first-order phase transitions starting from the shell configuration.[1]

It is worthwhile noticing that for the smallest tube radii, i.e., $R_t\leqslant 7$ Å, the film growth is always stable above the submonolayer condensation that takes place at low coverages. Instead, $R_t=8$ Å is peculiar due to the fact that the layer promotion that follows monolayer completion occurs in the unstable regime $d\mu/dn_4<0$. This can be visualized in the inset of Fig. 1. In this case, film growth happens discontinuously and a Maxwell construction yields the size Δn_4 of the jump in the order parameter. We find $\Delta n_4=0.55$ Å^{-1}, which in turn corresponds to $\Delta n_s=0.22$ layers for a radius

TABLE I. Energy of the bandheads for angular motion, centroids, root-mean-square distance to the axis, and dispersion of the wave functions for the radial ground-state band/$n=0$), in a cylinder with $R_t=7$ Å and $n_4=2.5$ Å . The position of the radial bandheads for $n=1$, 2, and 3 are shown at the bottom.

l	ε_{0l} [K]	$\varepsilon_{00}+\frac{\hbar^2\, l^2}{2mR_{shell}^2}$[K]	$\langle r\rangle$ [Å]	$r_{\rm rms}=\sqrt{\langle r^2\rangle}$ [Å]	w [Å]
0	−130.11	−130.11	4.07	4.08	0.27
1	−129.74	−129.74	4.07	4.08	0.27
2	−128.62	−128.65	4.07	4.08	0.27
3	−126.77	−126.83	4.07	4.08	0.27
4	−124.18	−124.27	4.07	4.08	0.27
5	−120.85	−120.99	4.08	4.09	0.27
6	−116.79	−116.98	4.08	4.09	0.27
7	−112.00	−112.24	4.09	4.09	0.27
8	−106.49	−106.77	4.09	4.10	0.26
9	−100.26	−100.57	4.10	4.10	0.26
10	−93.32	−93.65	4.10	4.11	0.26
11	−85.67	−85.99	4.11	4.11	0.25
12	−77.32	−77.61	4.11	4.12	0.25
13	−68.27	−68.49	4.12	4.13	0.25
14	−58.54	−58.65	4.13	4.13	0.25
15	−48.11	−48.07	4.13	4.14	0.24
n	ε_{n0} [K]				
1	−66.77				
2	−58.75				
3	−40.80				

[a]Width evaluated as $w=\sqrt{\langle r^2\rangle-\langle r\rangle^2}$.

$R_{shell}=5$ Å. Therefore, this is a phenomenon of discontinuous film growth similar to that occurring on planar graphite[18,20,21] and appears to be intrinsic to tube radii equal to or above 8 Å, for which inwards arrangement of helium takes place along a sequence of cylindrical shells, which are essentially two-dimensional configurations. The situation is different for the smaller radii, where monolayer completion is followed by the appearance of an axial state of one-dimensional nature. This suggests that the instability commented above is a feature of the two-dimensional geometry that disappears when the inner cylindrical shell shrinks into a line along the axis. The latter is, in fact, the most likely configuration in nanotube samples where the average radius is around 6.7 Å.[22]

Hereafter we concentrate our analysis on a pore with radius $R_t=7$ Å. In Table I we display the eigenenergies ε_{n0} for a linear density $n_4=2.5$ Å^{-1}, $n=0$–3. For the radial ground state band $n=0$, we also show in the first column the angular bandheads ε_{0l}, $l=0$–15. These values confirm the large- scale separation associated with the cylinder dimensions, the radial quantum $\varepsilon_{10}-\varepsilon_{00}=63.34$ K being a factor of 170 larger than the angular one, $\varepsilon_{01}-\varepsilon_{00}=0.37$ K. On the other hand, we verify that at least in the radial ground-state band, the thresholds for angular motion are almost indistinguishable from the free particle ansatz $\varepsilon_{0l}=\mu_4+\hbar^2\, l^2/(2mR_{shell}^2)$ shown in column 2 of Table I, where R_{shell} stands for the centroid of the ground-state density (cf. Fig. 2). The last three columns contain the values of the centroid of the density distribution, its rms, and variance. The numbers indicate that the density profiles depend very weakly on the angular motion; this can be viewed in Fig. 3, where the wave functions $f_{0l}(r)$ are plotted for l between 0 and 15. The relevant information from this drawing is the poor influence of the centrifugal potential in the vicinity of the walls, due to the large depth of the graphite field. This fact may introduce an important simplification for more complex problems— for example, studies of mixtures of he-

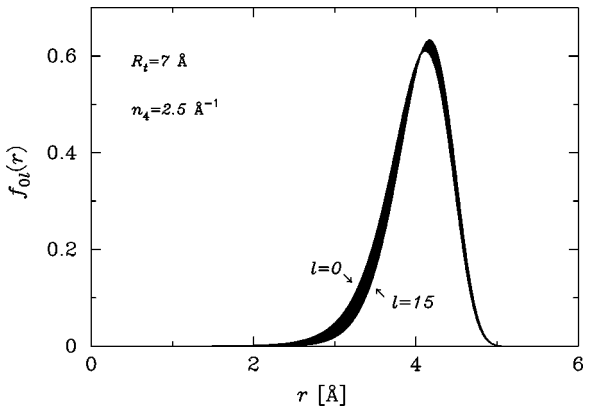

FIG. 3. Angular wave functions $f_{0l}(r)$ for the radial ground-state band in a cylinder with $R_t=7$ Å and $n_4=2.5$ Å^{-1}.

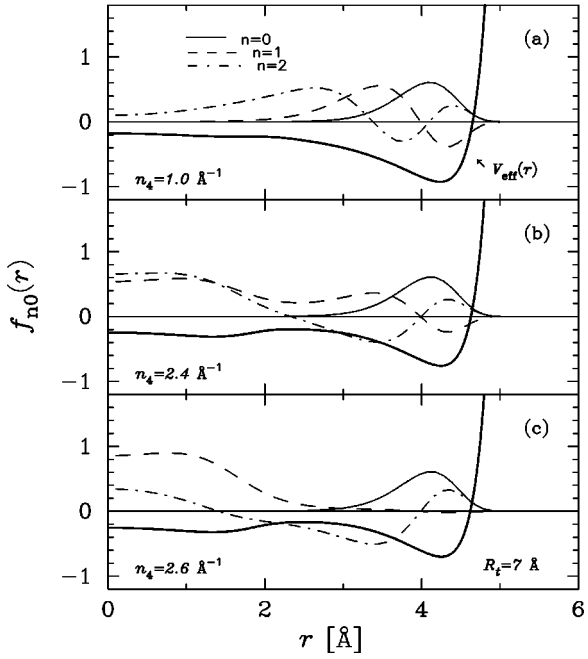

FIG. 4. Ground-state and first- and second-excited radial wave functions, together with the equilibrium mean field, in a cylinder with radius $R_t=7$ Å and for increasing linear density n_4.

lium isotopes which involve, in principle, the computation of a large amount of wave functions for the ^{3}He atoms—since the compression induced by the angular motion could be disregarded for a preliminary semiquantitative analysis.

In Figs. 4 and 5 we show, for a series of linear densities n_4, the normalized ground-state and first and second-excited radial wave functions $f_{00}(r)$, $f_{10}(r)$, and $f_{20}(r)$, together with the mean field potential, which corresponds to the equilibrium density ρ_4. Various important features of this structure should be pointed out. At first sight, the main peak in the

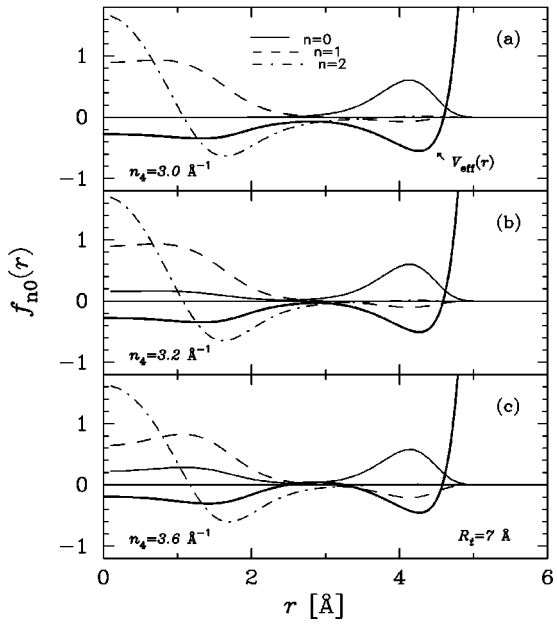

FIG. 5. Same as Fig. 4 for other values of n_4.

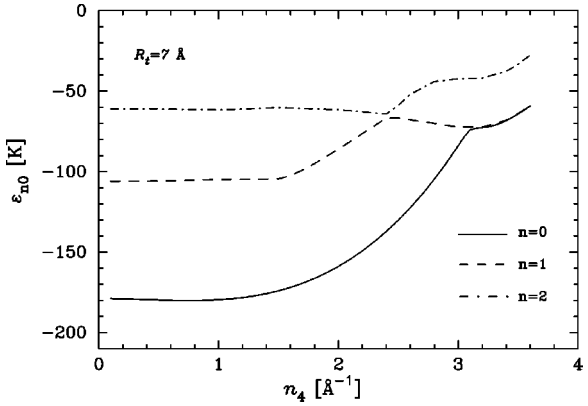

FIG. 6. Radial single-particle energies ε_{n0} for $R_t=7$ Å as functions of linear density n_4.

ground state is remarkably stable against increasing number of atoms. Apparently this is also the case for the first-excited radial state, at least at the lowest linear densities; however, slight distortions in the mean field, announcing the appearance of a secondary minimum at smaller radii, become evident in, i.e., the lowest panel of Fig. 4. This distortion becomes dramatic in the vicinity of the transition to the double-shell configuration and provokes an impressive change in the pattern of the excited states (cf. Fig. 5), which display as well a pronounced increase of the probability amplitude at the location of the secondary shell.

The behavior of the wave functions can be further understood in the light of Fig. 6, where we plot the energies ε_{n0} for $n=0$, 1, and 2 as functions of n_4. In fact, the upper energies undergo one Landau-Zener-like crossing, so that the corresponding states become almost degenerate at the given atom numbers. This is the case for ε_{00} and ε_{10} near the formation of the ''extended'' axial state at $n_4\simeq 3.1$ Å^{-1}, where the regime exhibits quasidegeneracy of the earlier radial ground state and first excited state in the equilibrium mean field. Moreover, this value of n_4 corresponds to a coverage $n_s=0.123$ Å^{-2}, thus in good quantitative agreement with the threshold for second-layer promotion observed in helium films on flat graphite surfaces.[23]

The probability density $|\psi_3(r)|^2$ of a single ^{3}He impurity adsorbed into the ^{4}He fluid is another topic of interest, since its behavior in the case of planar helium films adsorbed on graphite has been thoroughly investigated in the past.[24] This probability density is such that

$$2\pi \int r dr |\psi_3(r)|^2 = 1 \tag{2.9}$$

[cf. Eq. (2.2)]. In order to examine these density profiles in the current cylindrical geometry, we solve the Schrödinger equation for a single ^{3}He atom in the mean field given by the density functional description of mixtures of helium isotopes,[25–27] we set the particle and kinetic energy densities of the latter fluid equal to zero in the coupling contributions to the mean field experienced by this single atom. In Fig. 7 we plot the radial density $\rho_3(r)$ as a function of radial distance for various ^{4}He linear densities n_4. In this figure we can observe that at the lowest linear densities, the impurity

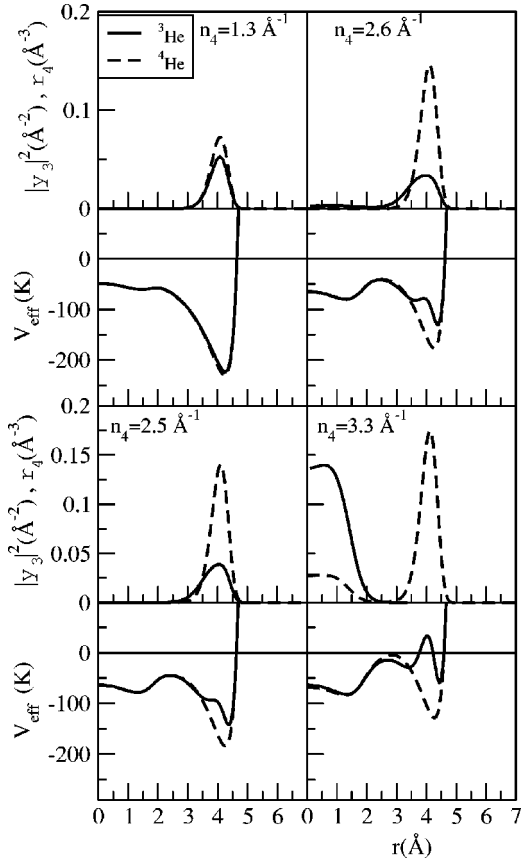

FIG. 7. Probability density of one ^{3}He impurity and particle density of the adsorbed ^{4}He fluid, together with the respective mean fields experienced by the atoms, for various linear densities n_4. Quantities $\rho(r)$ and $|\psi_3(r)||^2$ are normalized according to Eqs. (2.2) and (2.9).

remains confined to the interior of the adsorbed shell. Instead, the probability density is pushed inwards with increasing n_4 and becomes finally concentrated inside the inner shell. This evolution pattern is in qualitative agreement with the microscopic calculations for He on graphite of Ref. 24, where it has been shown that as the thickness of the films grows and layering sets in, the ^{3}He atom is expelled towards the free surface.

III. THERMODYNAMICS OF THE EXCITATIONS

Let us assume that the helium fluid exhibits well-defined collective excitation branches $\hbar\omega_\alpha(\lambda,q)$ corresponding to the response to external fields which transfer angular momentum λ and linear axial momentum q. Here α labels the various dispersion relations that may arise as roots of the secular equation—i.e., the RPA equation—for the collective modes.[28] The total energy of these excitation branches is computed as a function of temperature as

$$U(T)=\sum_{\alpha\lambda q}\hbar\omega_\alpha(\lambda,q)n[\hbar\omega_\alpha(\lambda,q)], \tag{3.1}$$

so that the specific heat reads, in terms of the Bose occupation numbers $n(\varepsilon)=1/[e^{\varepsilon/k_BT}-1]$,

$$\frac{C(T)}{N_4k_B}=\frac{1}{2\pi n_4}\sum_{\alpha\lambda}\int dq\left[\frac{\hbar\omega_\alpha(\lambda,q)}{k_BT}\right]^2 \times n[\hbar\omega_\alpha(\lambda,q)]\{1+n[\hbar\omega_\alpha(\lambda,q)]\}. \tag{3.2}$$

The pure phonon contribution to the specific heat of one cylindrical shell was previously examined in Ref. 14 for both liquid and solid ^{4}He, on very general grounds which suggested a thermodynamic means of determining the speed of sound in the given environment. A similar problem was addressed in Ref. 13, where it was assumed that very dilute helium atoms—i.e., at the saturation density $\tilde{n}_4=n_4/2\pi=0.036$ Å^{-1} of one-dimensional helium reported in previous works[9,10]—confined to a cylindrical surface of radius R_{shell}, interact with a contact force of constant strength g. The s.p. spectrum of these atoms is described by $\varepsilon_{\lambda q}=\hbar^2(q^2+\lambda^2/R_{shell}^2)/2m$. A single branch of excitations was encountered, corresponding to the Bogoliubov spectrum

$$[\hbar\omega(\lambda,q)]^2=\varepsilon_{\lambda q}^2+2gn_4\varepsilon_{\lambda q}. \tag{3.3}$$

In this case, the specific heat of a single cylindrical shell displays not only the dimensionality crossover from one to two dimensions as higher-angular-momentum bands become excited, but the transition between phononlike and particlelike behavior of boson excitations in this particular environment.

As discussed in the previous section, in the realistic geometry and energy configurations which make room to transverse motion of the atoms, the first excited radial band lies at very high energies provided that the number of helium atoms remains below, say, 3 Å^{-1}. When transverse s.p. states become competitive with the angular bandheads, at linear densities close to the formation of the second shell, transitions that change the number of radial nodes cannot be disregarded. In order to analyze the subsequent modifications to the simplified scenarios in Refs. 13 and 14, we start by assuming that the s.p. spectrum of the ^{4}He quasiparticles in the mean field can be represented by the simplified expression

$$\varepsilon_{nlk}\equiv\varepsilon_{nl}+\varepsilon_k =\varepsilon_n+\frac{\hbar^2l^2}{2mR_{shell}^2}+\frac{\hbar^2\ k^2}{2m} \tag{3.4}$$

(cf. Table I). Furthermore, we assume that the ground state is excited by an operator which, in addition to being able to create n radial nodes, transfers axial momentum q and angular momentum λ, of the form

$$O(\mathbf{r})=O_{n\lambda}(r)e^{i(qz+\lambda\varphi)}. \tag{3.5}$$

The RPA secular equation can be solved analytically when the radial excited band lies sufficiently high in energy, typically for low linear densities of helium atoms. The RPA susceptibility reads

$$\chi_{0\lambda q}^{RPA}(\omega)=\chi_{0\lambda q}^0(\omega)+\chi_{0\lambda q}^0(\omega)V_{0\lambda q}\chi_{0\lambda q}^{RPA}(\omega), \tag{3.6}$$

being

$$\chi^0_{0\lambda q}(\omega) = |\langle 0\lambda|O_{0\lambda}|00\rangle|^2 \tilde{n}_4 \times \left[\frac{1}{\hbar\omega - \varepsilon_{0\lambda q} + i\eta} - \frac{1}{\hbar\omega + \varepsilon_{0\lambda q} + i\eta}\right] \tag{3.7}$$

and

$$V_{0\lambda q} = \langle 000, 0\lambda q|V_{ph}|0\lambda q, 000\rangle, \tag{3.8}$$

where $V_{ph}(\mathbf{r}, \mathbf{r}')$ is the effective particle-hole (ph) interaction, which in the density functional frame is computed as the double-functional derivative of the total energy with respect to the local particle density. The eigenfrequencies of the collective modes in Eq. (3.6) are the zeros of the dielectric function $\epsilon(q,\lambda,\omega) = 1 - \chi^0_{0\lambda q}(\omega) V_{0\lambda q}$, which reproduce the RPA-Bogoliubov branches [cf. Eq. (3.3)]

$$[\hbar\omega_0(\lambda,q)]^2 = \varepsilon^2_{0\lambda q} + 2\tilde{n}_4 V_{0\lambda q} |\langle 0\lambda|O_{0\lambda}|00\rangle|^2 \varepsilon_{0\lambda q}. \tag{3.9}$$

For low enough linear densities, the radial bands lie sufficiently apart and uncoupled α branches [cf. Eq. (3.2)] appear associated with the quantum number n, with dispersion relations $[\hbar\omega_n(\lambda,q)]^2$ obtained from Eq. (3.9) upon substitution of the radial quantum number 0 into n. As discussed in the preceding section, when n_4 increases the ground state (g.s.) and first excited radial energies undergo opposite trends and approach each other (cf. Fig. 6), thus enlarging the domain for ph propagation and coupling the different RPA branches.

Since our goal is to shed light on the possible evolution of the spectrum and the heat capacity, in connection with the energy gap for transverse motion, our calculations are exploratory and have been performed under substantial simplifications. In particular, we focus on an adequate description of the phonon branch, consistent with the equation of state depicted in Fig. 1; consequently, we select, at each linear density for all λ and q, the interaction strength $g_0 = V_{000} |\langle 0\lambda|O_{0\lambda}|00\rangle|^2$ that reproduces the sound velocity derived from $E(n_4)$ (cf. Fig. 1) in the stable regime, i.e., for linear densities roughly above 1 Å^{-1}. Similarly, one could derive a parameter $g_1 = V_{100} |\langle 1\lambda|O_{0\lambda}|10\rangle|^2$ from the slope of the curve $\varepsilon_{10}(n_4)$ and compute the Bogoliubov branch associated to the s.p. energy $\varepsilon_{1\lambda q}$. This criterion for the choice of g_1 cannot be applied in the interval 2.4 Å$^{-1} \leqslant n_4 \leqslant 3.1$ Å^{-1} where the slope of $\varepsilon_{10}(n_4)$ is negative. However, below the Landau-Zener crossing between $\varepsilon_{10}(n_4)$ and $\varepsilon_{20}(n_4)$ near $n_4 \simeq 2.4$ Å^{-1}, these constants are so similar that no quantitative changes can be reported if we choose all matrix elements to be identical.

We adopt this simple scheme at all linear densities, for the purpose of qualitative comparison, and consider the phonon specific heat in Eq. (3.2) for different situations, as shown in Fig. 8, where we display $C/(N_4 k_B)$ as a function of temperature T (in K) for various linear densities n_4 above 1 Å^{-1}. In this temperature range, the thermal cutoff to the integral (3.2) introduced by the Bose occupation numbers secures that essentially the phonon branch—i.e., $q < 0.5$ Å^{-1}—is being included.

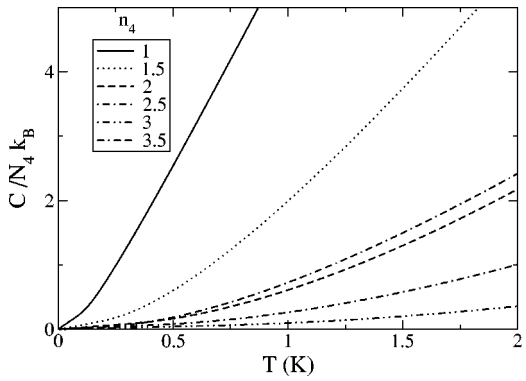

FIG. 8. Specific heat of the phonon branches of the excitation spectrum as a function of temperature for various linear densities.

The general feature in this plot is that at sufficiently low temperatures, i.e., $T \lesssim 0.1$ K, all these curves are linear functions of T, showing the predominant 1D phononlike origin of the specific heat,[11,14] according to the rule

$$\frac{C_{1D}}{N k_B} = \frac{\pi}{3 n_4 \hbar c_s} k_B T. \tag{3.10}$$

Moreover, all curves experience a change in slope indicative of a crossover to a Q1D regime where excitations with nonvanishing angular momentum participate in thermal activity. The overall quenching of the specific heat is mostly governed by the $1/(n_4 c_s)$ slope [cf. Eq. (3.2)]; anyway, nonmonotonic behavior of the slope dC/dT as a function of n_4 becomes visible above $n_4 = 2$ Å^{-1}. Correspondingly, the isotherms C_{1D} vs n_4 display "dips" reminiscent of those reported in the case of planar films[23] at the various phase transitions that take place in the first layer. In fact, a previous investigation of the dimensional crossover of the phonon specific heat liquid and solid ^{4}He in a single cylindrical shell was carried out in Ref. 14, where emphasis was laid on the excitation of the angular-plus-linear momentum branches $\hbar^2 l^2/(2mR^2_{shell}) + \hbar^2 k^2/(2m)$ on the g.s. band $n = 0$. While in this work it was argued that a measurement of the phonon heat capacity would shed light on the value of the speed of sound, the present approach derives these values from the equation of state and from the density dependence of the excited transverse bandhead ε_{10}.

A word of caution concerning the specific heat should, however, be stated, since within the range of linear densities being considered, the first shell of ^{4}He atoms is expected to be solid.[23] In fact, the phase diagram of ^{4}He films on flat graphite surfaces indicates the presence of a commensurate solid—eventually coexisting with a fluid phase—or an incommensurate solid for areal coverages between 0.04 and 0.12 Å^{-2}, which corresponds to n_4 between 1.005 and 3.015 Å^{-1} on a perfect cylindrical surface with a radius R_{shell} of 4 Å. The present results on excitation spectra and specific heat of helium atoms actually correspond to a high- density fluid. In this description, the values for the coupling con-

stants and sound velocities of the first and second shells were extracted from the EOS. As a consequence, we predict reference values for the phonon specific heat of a homogeneous fluid in the cylindrical geometry, at the density of the expected solid layer, which should be confronted with future measurements to assert the validity of the Debye model for this solid.

IV. SUMMARY AND CONCLUSIONS

In this work, we have performed a systematic calculation of the structure and elementary and phonon excitations of quantum fluid ^{4}He adsorbed in the interior of carbon nanotubes, employing a description based on a finite-range density functional. In Sec. II, it has been concluded that the structure of the helium fluid inside the cylinder evolves with the number of atoms as does the liquid adsorbed on a flat graphite surface, presenting a layering transition at linear densities which, for different tube radii, reproduce the value of the areal coverage for first-layer promotion encountered in planar films. Some indications of this behavior were anticipated in Ref. 3, where, however, the emphasis was laid on the appearance of the axial state. We may then say that this structure would correspond to a ''rolled-up'' helium film grown on a graphene sheet; further confirmation of this tendency is provided by the behavior of a single ^{3}He impurity diluted into the adsorbed host. This result is far from trivial; in fact, since the radial potential of graphite seen by the adatoms in the interior of a nanotube seems to strengthen its attraction as curvature increases,[17] one might have expected more substantial quantitative modifications to the film pattern.

We have also presented a simple description of the lowest excitation modes of the adsorbed fluid and computed the low-temperature contribution of the phonon spectrum to the specific heat, which displays the dimensionality characteristics already reported[13] in the very dilute limit. In the present case, the range of linear densities rather corresponds to the solid first layer encountered in flat helium films on graphite. The excitations and subsequent specific heat data should then be regarded as a phenomenological picture of the phonon spectrum of the 1D harmonic solid subjected to anharmonic coupling.[29]

ACKNOWLEDGMENTS

This work was performed under Grant No. X103 from University of Buenos Aires. We are pleased to acknowledge useful comments from Manuel Barranco and helpful discussions with Mercedes M. Calbi and Milton W. Cole.

[1] M. M. Calbi, M. W. Cole, S. M. Gatica, M. J. Bojan, and G. Stan, Rev. Mod. Phys. **73**, 857 (2001).
[2] M. W. Cole, V. H. Crespi, G. Stan, C. Ebner, J. M. Hartman, S. Moroni, and M. Boninsegni, Phys. Rev. Lett. **84**, 3883 (2000).
[3] S. M. Gatica, G. Stan, M. M. Calbi, J. K. Johnson, and M. W. Cole, J. Low Temp. Phys. **120**, 337 (2000).
[4] G. Stan, M. J. Bojan, S. Curtarolo, S. M. Gatica, and M. W. Cole, Phys. Rev. B **62**, 2173 (2000).
[5] S. M. Gatica, M. W. Cole, G. Stan, J. M. Hartman, and V. H. Crespi, Phys. Rev. B **62**, 9989 (2000).
[6] L. Szybisz and S. M. Gatica, Phys. Rev. B **64**, 224523 (2001).
[7] S. M. Gatica, M. M. Calbi, and M. W. Cole, Phys. Rev. E **65**, 061605 (2002).
[8] L. Szybisz and I. Urrutia, Phys. Rev. E **66**, 051201 (2002).
[9] E. Krotscheck and M. D. Miller, Phys. Rev. B **60**, 13 038 (1999).
[10] M. Boninsegni and S. Moroni, J. Low Temp. Phys. **118**, 1 (2000).
[11] E. S. Hernández and M. W. Cole, J. Low Temp. Phys. **126**, 217 (2002).
[12] E. S. Hernández, J. Low Temp. Phys. **127**, 153 (2002).
[13] E. S. Hernández, Phys. Rev. Lett. **89**, 185301 (2002).
[14] A. M. Vidales, V. H. Crespi, and M. W. Cole, Phys. Rev. B **58**, R13 426 (1998).
[15] R. A. Trasca, A. M. Vidales, and M. W. Cole, cond-mat/0211172.
[16] F. Dalfovo, A. Lastri, L. Pricaupenko, S. Stringari, and J. Treiner, Phys. Rev. B **52**, 1193 (1995).
[17] G. Stan and M. W. Cole, Surf. Sci. **395**, 280 (1998).
[18] E. Krotscheck, Phys. Rev. B **32**, 5713 (1985).
[19] E. Cheng, M. W. Cole, W. F. Saam, and J. Treiner, Phys. Rev. B **46**, 13 967 (1992).
[20] B. E. Clements, E. Krotscheck, and H. J. Lauter, Phys. Rev. Lett. **70**, 1287 (1993).
[21] B. E. Clements, J. L. Epstein, E. Krotscheck, and M. Saarela, Phys. Rev. B **48**, 7450 (1993).
[22] A. G. Rinzler *et al.*, Appl. Phys. A: Mater. Sci. Process. **67**, 29 (1998).
[23] D. S. Greywall, Phys. Rev. B **47**, 309 (1993).
[24] E. Krotscheck, M. Saarela, and J. L. Epstein, Phys. Rev. B **38**, 111 (1988).
[25] M. Barranco *et al.*, Phys. Rev. B **56**, 8997 (1997).
[26] M. Pi, R. Mayol, and M. Barranco, Phys. Rev. Lett. **82**, 3093 (1999).
[27] R. Mayol, M. Pi, M. Barranco, and F. Dalfovo, Phys. Rev. Lett. **87**, 145301 (2001).
[28] This label should not be mistaken by the number of nodes of the s.p. radial wave function; more generally, one may expect α to reflect the number of nodes of a density fluctuation of given multipolarity λ and transferred momentum q.
[29] H. R. Glyde, *Excitations in Liquid and Solid Helium* (Clarendon Press, Oxford, 1994).